JACS
JOURNAL OF THE AMERICAN CHEMICAL SOCIETY
Article
pubs.acs.org/JACS

Crystal and Electronic Structures of Neptunium Nitrides Synthesized Using a Fluoride Route

G. W. Chinthaka Silva,*[,†,‡] Philippe F. Weck,[§] Eunja Kim,[∥] Charles B. Yeamans,[⊥] Gary S. Cerefice,[#] Alfred P. Sattelberger,[▽] and Kenneth R. Czerwinski[†,§]

[†]Harry Reid Center for Environmental Studies, University of Nevada, Las Vegas, Box 454009, 4505 Maryland Parkway, Las Vegas, Nevada 89154, United States

[‡]Nuclear Fuel Materials Group, Fuel Cycle & Isotopes Division, Oak Ridge National Laboratory, Oak Ridge, Tennessee 37831-6093, United States

[§]Sandia National Laboratories, Advanced Systems Analysis, P.O. Box 5800, Albuquerque, New Mexico 87185-0779, United States

[∥]Department of Physics and Astronomy, University of Nevada, Las Vegas, Box 454002, 4505 Maryland Parkway, Las Vegas, Nevada 89154, United States

[⊥]Chemical Sciences Division, Lawrence Livermore National Laboratory, 7000 East Avenue, L-550, Livermore, California 94551, United States

[#]Department of Health Physics and Diagnostic Sciences, University of Nevada, Las Vegas, Las Vegas, Nevada 89154, United States

[▽]Energy Engineering and Systems Analysis Directorate, Argonne National Laboratory, Argonne, Illinois 60439, United States

Supporting Information

ABSTRACT: A low-temperature fluoride route was utilized to synthesize neptunium mononitride, NpN. Through the development of this process, two new neptunium nitride species, NpN_2 and Np_2N_3, were identified. The NpN_2 and Np_2N_3 have crystal structures isomorphous to those of UN_2 and U_2N_3, respectively. NpN_2 crystallizes in a face-centered cubic CaF_2-type structure with a space group of $Fm\bar{3}m$ and a refined lattice parameter of 5.3236(1) Å. The Np_2N_3 adopts the body-centered cubic Mn_2O_3-type structure with a space group of $Ia\bar{3}$. Its refined lattice parameter is 10.6513(4) Å. The NpN synthesis at temperatures ≤900 °C using the fluoride route discussed here was also demonstrated. Previous computational studies of the neptunium nitride system have focused exclusively on the NpN phase because no evidence was reported experimentally on the presence of NpN_x systems. Here, the crystal structures of NpN_2 and Np_2N_3 are discussed for the first time, confirming the experimental results by density functional calculations (DFT). These DFT calculations were performed within the local-density approximation (LDA+U) and the generalized-gradient approximation (GGA+U) corrected with an effective Hubbard parameter to account for the strong on-site Coulomb repulsion between Np 5f electrons. The effects of the spin−orbit coupling in the GGA+U calculations have also been investigated for NpN_2 and NpN.

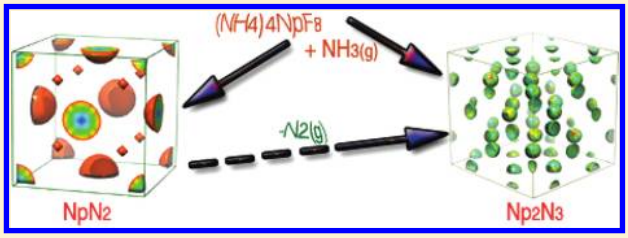

1. INTRODUCTION

Nitride fuel matrixes are often considered as alternatives to oxide fuels for applications where a higher fissile-atom density is required, such as fast reactor systems. For these systems, nitride fuel matrixes provide a valuable midpoint between the superior mechanical and thermodynamic fuel properties of the oxides and the low light-atom density and high thermal conductivity of metallic fuels.[1−3] Nitride matrixes also offer superior mutual solubility between the actinides[4] as compared to metal alloy systems,[5] and the thermodynamic properties of the mixed actinide nitrides are readily predictable based on those from their constituent binary species.[6,7] Closed fuel cycles based on a nitride fuel matrix are largely similar to the recycling of oxide fuels, but with the distinct advantage of easier fuel element dissolution.[8]

Mixed actinide nitride and carbo-nitride matrixes[9] have also been considered as target materials for accelerator-driven subcritical systems (ADS), either as stand alone target materials or in an inert ZrN matrix.[10] The Japan Atomic Energy Research Institute (JAERI) considers nitrides to be a top fuel-material candidate for its accelerator-driven systems for minor actinide transmutation.[11] Minor actinide transmutation is a key component of the double-strata fuel cycle proposed by JAERI,[12] and a nitride fuel form is considered acceptable for this purpose. Nitride fuels are ideal for space reactor applications because of their superior performance at high burnup and high temperatures.[13,14] In particular, nitride fuels

Received: October 17, 2011
Published: January 26, 2012

   dx.doi.org/10.1021/ja209503n | J. Am. Chem. Soc. 2012, 134, 3111−3119

retain their hardness at high temperatures much better than their primary alternative, uranium carbide (UC).[15]

A fluoride-based route was utilized for the synthesis of UN[16,17] as part of previous work examining the actinide nitride system. As compared to the other synthetic routes available, the fluoride-based synthetic route for the actinide nitrides offers a number of potential advantages, primarily the reduction in processing temperatures and the elimination of carbide contamination of the product. Synthesis of the mononitride at low temperatures is the most important advantage of this route because it minimizes oxide content and completely eliminates carbide contamination common in fuel made using the carbothermic reduction process. The most commonly used method to fabricate actinide mononitrides is the carbothermic reduction,[18] and it has been used to synthesize NpN as well.[19] Using carbothermic reduction of NpO_2, NpN could be synthesized after heating to 1550 °C for 10 h. Alternatively, NpN can be synthesized by reacting Np metal with a N_2/H_2(0.5%) gas mixture at 600 °C.[20] Sheft and Fried[21] reported the synthesis of NpN using NpH_3 with NH_3 vapor at 750−775 °C and reported NpN to be isostructural to UN and PuN. An attempt to produce NpN by a reaction of $NpCl_4$ with NH_3(g) at 350−400 and 1000 °C instead formed $NpCl_3$.

To the best of our knowledge, NpN is the only neptunium nitride phase identified experimentally so far. This appears particularly surprising because actinide mononitrides AnN (An = Ac, Th, Pa, U, Np, Pu, Am) are all isostructural (NaCl-type structure, space group $Fm\bar{3}m$, IT no. 225), and the phase diagram of the U−N system shows the existence of at least three additional phases, that is, α-U_2N_3 (body-centered cubic Mn_2O_3-type structure, space group $Ia\bar{3}$, IT no. 206) and UN_2 (face-centered cubic CaF_2-type structure, space group $Fm\bar{3}m$, IT no. 225) at temperatures below ca. 1323 °C and β-U_2N_3 (trigonal La_2O_3-type structure, space group $P\bar{3}1$, IT no. 164) at higher temperatures; other UN_x (x = 1.45−1.90) stoichiometries were also reported.[22] Previous computational studies of the neptunium nitride system have focused exclusively on the NpN phase[23−28] because no evidence was reported experimentally on the presence of NpN_x systems.

In this study, we report the existence of two new neptunium nitride phases, NpN_2 and Np_2N_3, identified in the process of synthesizing neptunium mononitride using the low-temperature fluoride route. Synthesis of NpN via the fluoride route will also be briefly discussed as further experimentation is required to optimize the experimental conditions for the synthesis of single-phased NpN. The crystal structures of these phases have been also confirmed by density functional calculations performed within the local-density approximation (LDA+U) and the generalized-gradient approximation (GGA +U) corrected with an effective Hubbard parameter. Experimental and computational methods used in this study are given in section 2, followed by results in section 3 and a discussion of our findings and conclusions in section 4.

2. EXPERIMENTAL AND COMPUTATIONAL METHODS

2.1. Synthesis of the Ammonium Neptunium Fluorides: NH_4−Np−F. The ammonium neptunium fluoride starting materials for the low-temperature fluoride route to synthesize neptunium nitrides were made by mixing solid neptunium oxide ($^{237}NpO_2$) with solid ammonium bifluoride (NH_4HF_2) in a Teflon bottle at a 4.2:1 NH_4HF_2:NpO_2 molar ratio. All of the powder manipulations were performed inside a glovebox. The solids inside the bottle were then mixed with a spatula for 10 min. The product NH_4−Np−F samples were used in the next step described in section 2.2. (Caution: Np-237 is a radioactive isotope and should be handled carefully with appropriate safety measures applied.)

2.2. Ammonolysis of Ammonium Neptunium Fluoride. The ammonium neptunium fluoride samples in platinum containers/foils were placed in quartz heating tube. The reactants were enveloped using Pt sheets to prevent further oxidation of any nitride products formed during the ammonolysis. Metallic zirconium placed on Pt containers was used as oxygen getters inside the heating tubes at both upstream and downstream locations. These sample preparations were carried out in a similar way as in the case of UN synthesis,[29] where more than 97 wt % single-phased nitrides were synthesized.[17] Because of the radiological concerns of the neptunium-bearing samples and the limited quantities available, a mass less than 30 mg of the NH_4−Np−F sample was used in each of these experiments. The conversion reactions of the fluorides into nitrides were carried out under ammonia gas (Grade 4.5) at temperatures from 250 to 1100 °C. Extensive experimentations were performed at 800 °C because it was found to be the optimal temperature for other ammonium uranium fluorides conversion into the nitrides.[16] Time of heating was varied from 30 to 120 min. Use of these different experimental conditions is described in the Results as fitting. NpN_2 samples were made using closed Pt containers, while Np_2N_3 samples were made in open Pt containers. Note that all of the experimental works were carried out at the University of Nevada, Las Vegas, NV.

2.3. Conversion of Higher Nitrides into the Mononitride. Further reduction of the higher nitrides synthesized in the ammonolysis step was carried out under high-purity (99.999%) argon and/or Ar/H_2(4%) atmosphere. These conversions were tested at three different temperatures, 800, 900, and 1100 °C, and 30−60 min of heating time.

2.4. Characterization by X-ray Powder Diffraction (XRD). Chemical phase identification in the synthesized samples was performed using powder XRD patterns. The as-synthesized samples were prepared for XRD runs by adding the powder samples onto a zero-background silicon wafer. The sample holder was then sealed with a Kapton tape inside a glovebox. All of the XRD patterns were obtained using a Philips PANalytical X'Pert Pro instrument with a Cu K_α ($K_{\alpha1}$ and $K_{\alpha2}$) target and a Ni filter to filter out K_β radiation, using 40 mA current and 45 kV voltage. Structure refinements were performed by the Rietveld method using GSAS.[30] The initial estimates of the structural parameters used as a starting point for the structural refinements were based on structures available for the uranium nitride system in the Inorganic Crystal Structure Database (ICSD). Crystallographic parameters of UN_2 (ICSD #24222) and U_2N_3 (ICSD #24221) were used for NpN_2 and Np_2N_3, respectively. Jana 2000 software[31] was used to extract the structure factor amplitudes of the analyzed crystal systems using Le Bail decomposition.[32] The electron density maps of the synthesized materials were calculated using the charge flipping technique (Superflip[33]), and UCSF Chimera[34] was used to visualize them.

2.5. Density Functional Theory Calculations. First-principles total-energy calculations were performed using the spin-polarized density functional theory (DFT) as implemented in the Vienna ab initio simulation package (VASP).[35] The exchange-correlation energy was calculated within the local-density approximation (LDA+U) and the generalized gradient approximation (GGA+U), with the parametrizations of Perdew and Wang (PWC and PW91),[36,37] corrected with an effective Hubbard parameter, U_{eff}, to account for the strong on-site Coloumb repulsion between localized Np 5f electrons. Specifically, the formalism developed by Dudarev et al.[38] was used, which consists of adding a penalty functional to the standard LDA (or GGA) total-energy functional, E_{LDA}, which forces the on-site occupancy matrix in the direction of idempotency, that is:

$$E_{LDA+U} = E_{LDA} + \frac{(\bar{U} - \bar{J})}{2} \sum_{\sigma} [\mathrm{Tr}(\rho^{\sigma}) - \mathrm{Tr}(\rho^{\sigma}\rho^{\sigma})]$$

where $\bar{U}$ and $\bar{J}$ are the spherically averaged matrix elements of the screened electron−electron Coulomb and exchange interactions, respectively, and ρ^{σ} is the density matrix of f electrons with a given

projection of spin σ. In Dudarev's approach, only $U_{eff} = \bar{U} - \bar{J}$ is meaningful; therefore, $\bar{J}$ was set to 0.6 eV, a typical value for Np,[39] and only $\bar{U}$ was allowed to vary in the calculations.

The interaction between valence electrons and ionic cores was described by the projector augmented wave (PAW) method.[40,41] The Np (6s,7s,6p,6d,5f) and N (2s,2p) electrons were treated explicitly as valence electrons in the Kohn–Sham (KS) equation, and the remaining core electrons together with the nuclei were represented by PAW pseudopotentials. The KS equation was solved using the blocked Davidson iterative matrix diagonalization scheme followed by the residual vector minimization method. The plane-wave cutoff energy for the electronic wave functions was set to a value of 500 eV, ensuring the total energy of the system to be converged to within 1 meV/atom. Electronic relaxation was performed with the conjugate gradient method accelerated using the Methfessel–Paxton Fermi-level smearing[42] with a Gaussian width of 0.1 eV. Ionic relaxation was carried out using the quasi-Newton method, and the Hellmann–Feynman forces acting on atoms were calculated with a convergence tolerance set to 0.01 eV/Å. In the structural optimization and total-energy calculations, the Brillouin zone was sampled using the Monkhorst–-Pack special k-point scheme[43] with a 9 × 9 × 9 mesh for NpN and NpN_2 and a 3 × 3 × 3 mesh for Np_2N_3. A periodic supercell approach was used in the calculations with simulations cells containing 8, 12, and 80 atoms for NpN (Z = 4), NpN_2 (Z = 4), and Np_2N_3 (Z = 16), respectively. Ionic and cell relaxations were performed without symmetry constraints starting from the structures elucidated experimentally. In all magnetic calculations, the quantization axis for magnetization was chosen along the z-axis, coinciding in this study with the [111] crystallographic direction experimentally observed for the magnetization axis of NpN.[44]

Finally, following a computational approach similar to that described above to obtain collinear magnetic solutions, GGA+U calculations including the spin–orbit coupling (SOC) were also performed to investigate possible fully noncollinear magnetic structures of NpN and NpN_2.

3. RESULTS AND DISCUSSION

3.1. Synthesis and Characterization of NpN_2. Ammonolysis of the reactant ammonium neptunium fluorides, at temperatures below 800 °C, produced ammonium neptunium fluorides of different compositions and neptunium fluorides (Table 1). The absence of any NpO_2 in these samples also confirmed the complete conversion of reactant NpO_2 into the corresponding NH_4–Np–F, which was used in the ammonolysis. Neptunium fluorides and neptunium nitride fluorides were observed at 800 °C for a heating time of 60 min. Formation of a new neptunium nitride species, NpN_2, was identified when the heating time was increased to 90 min at 800 °C. The majority of this sample contained unreacted fluorides in the form of NpN_xF_y, which indicated a partial conversion reaction at these conditions. A third phase, NpO_2, was also found in this sample.

Table 1. Heating Ammonium Neptunium Fluorides under NH_3(g)

temp (°C)	time (min)	open or closed container	products (wt %)		
250	60	closed	$(NH_4)_2NpF_6$ (66.73)	NH_4NpF_5 (33.27)	
400	60	closed	$NH_4Np_3F_{13}$ (93.7)	NpO_2 (6.3)	
500	30	open	NpF_3 (75.0)	NpO_2 (25.0)	
800	60	closed	NpF_3 (3.8)	NpNF (96.2)	
800	90	closed	NpNF (72.7)	NpN_2 (15.9)	NpO_2 (11.4)
800	90	open	Np_2N_3 (51.4)	NpO_2 (45.5)	
800	120	closed	NpN_2 (81.1)	NpO_2 (18.9)	
1100	75	closed	NpN_2 (23.7)	NpO_2 (76.3)	

Another sample was made at 800 °C heating for 120 min in a closed container. A higher heating time was selected to achieve a full conversion of fluorides into nitrides. The resulting sample was primarily the nitride, NpN_2, with NpO_2 as the main contaminant phase (Table 1). A few other samples were made at higher temperatures, but a single-phased NpN_2 could not be synthesized. This is likely due to the extremely small sample sizes used for these reactions (approximately 20 mg per experiment), resulting in even minute quantities of oxygen in the system producing significant yields of the oxide phases. However, the XRD powder analysis was not affected by the presence of the second oxide phase (18.9 wt %) (Figure 1a) because the two XRD patterns were well separated, allowing proper analysis using the Rietveld method (χ^2 = 0.73).

Rietveld analysis of the XRD patterns showed that NpN_2 crystal structure is isomorphous to the cubic UN_2 with a space group of $Fm\bar{3}m$. The refined lattice parameter and the unit cell volume of NpN_2 were 5.3236(1) Å and 150.871(5) Å^3, respectively. A complete set of crystallographic details of the new compound can be found in Table 2. In its face-centered cubic unit cell, there are 14 identical lattice points (8 at corners of the cube and 6 in the centers of the six faces) corresponding to Np atoms. There are eight more identical lattice points in the unit cell corresponding to the N atoms (Figure 1b). Within one unit cell, each of the 6 Np atoms at the 6 face centers forms bonds with four neighboring N atoms defining 6 coordination polyhedra at refined Np–N bond distance of 2.30517(4) Å and two N–Np–N angles of 70.5289(2)° and 109.471(1)°. The calculated electron densities of NpN_2 using charge flipping method shown in Figure 1c also correlate well with the atomic sites of the refined unit cell (Figure 1b).

3.2. Synthesis and Characterization of Np_2N_3. Because the ammonium–neptunium fluoride (NH_4–Np–F) conversion at 800 °C and 90 min heating in a closed container produced NpN_2 and some unreacted NpN_xF_y, another sample was made using an open container with the same temperature and time of heating. By using an open container, it was expected to influence the reaction kinetics by increasing the level of hot inert gas flow passing through the sample particle surfaces. In this sample, all of the fluoride chemical phases converted into nitrides, forming another novel neptunium nitride, Np_2N_3, instead of NpN_2. The possible explanation for the formation of this low-stoichiometric nitride phase was the influence of the inert atmosphere on the NH4–Np–F decomposition at the used temperature. This sample also consisted of a considerable amount of secondary oxide phase due to the experimental factors discussed earlier in the case of NpN_2 synthesis.

XRD powder pattern analysis using Rietveld method was successfully performed on the Np_2N_3 phase (Figure 2a) with a χ^2 value of 0.93. It was shown that this compound has crystal structure isomorphous to that of U_2N_3 (ICSD #24221). The structure parameters obtained for Np_2N_3 are given in Table 2. It crystallizes in a cubic unit cell with $Ia\bar{3}$ space group. The lattice parameter is 10.6513(4) Å, and the unit-cell volume is 1208.4(1) Å^3. With a large unit cell, the Np_2N_3 has a complex atomic coordination system (Figure 2b). There are 44 lattice points corresponding to two neptunium atom environments,

dx.doi.org/10.1021/ja209503n | J. Am. Chem. Soc. 2012, 134, 3111–3119

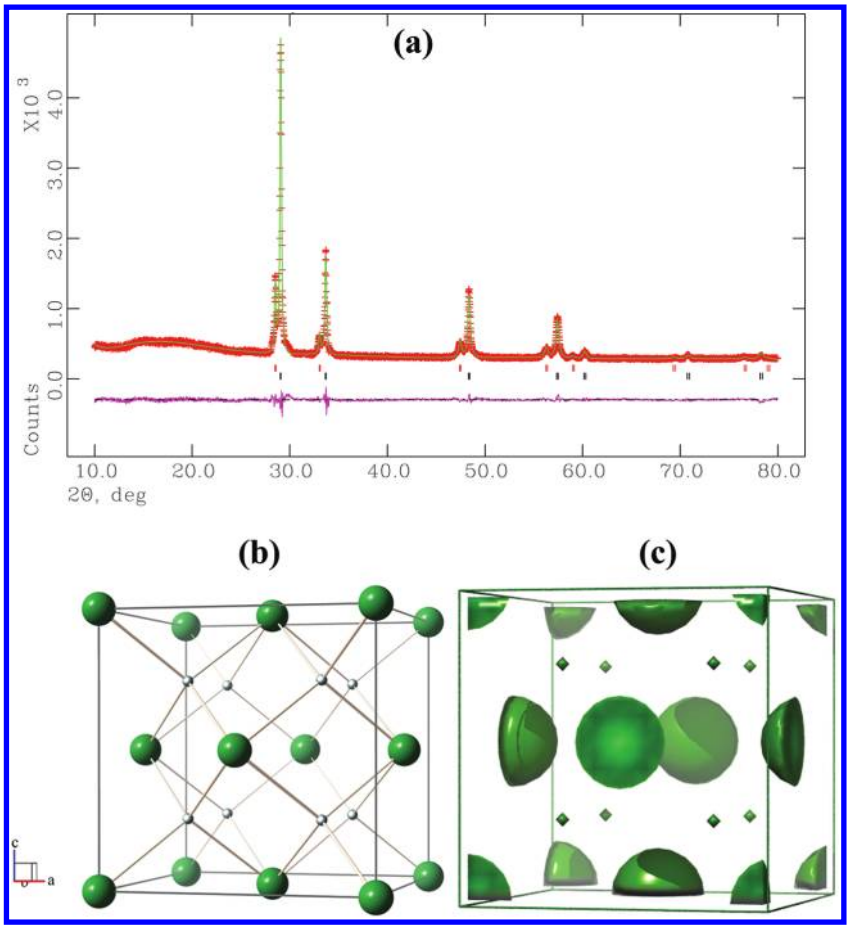

Figure 1. (a) Rietveld analysis of the NpN_2 powder XRD pattern (NpN_2 = 81.1 wt %, NpO_2 = 18.9 wt %, and χ^2 = 0.73). The red and green patterns represent the experimental pattern and the calculated fit, respectively. The pink color pattern at the bottom is the difference between the experimental and the fitted patterns. The lower tick marks (black) represent reflections corresponding to NpN_2, while upper ones are of NpO_2. The large and amorphous-type broad peak at low 2θ of the XRD pattern was due to the Kapton tape used to seal the sample. (b) A ball-and-stick model of the refined NpN_2 unit cell. (c) Electron density map of NpN_2 unit cell (level of display = 4.82).

Table 2. Crystallographic Data of NpN_x

				compound			
				NpN_2	Np_2N_3	NpN	
space group				$Fm\bar{3}m$ (cubic)	$Ia\bar{3}$ (cubic)	$Fm\bar{3}m$ (cubic)	
a (Å)				5.3236(1)	10.6513(4)	4.8999(1)	
$\alpha = \beta = \gamma$				90	90	90	
cell volume (Å^3)				150.871(5)	1208.4(1)	117.64(1)	
density (g cm^{-3})				11.692	11.348	14.174	
cell formula units (z)				4	16	4	
wRp (%)				3.72	7.72	5.97	
Rp (%)				2.82	5.78	3.83	
χ^2				0.73	0.93	2.20	
atom	x	y	z	frac	U_{iso} (Å^2)	site sym	multiplicity
				NpN_2			
Np	0	0	0	1	0.0708(5)	$m3m$	4
N	0.25	0.25	0.25	1	0.022(3)	$-43m$	8
				Np_2N_3			
Np(1)	0.25	0.25	0.25	1	0.011(2)	$-3(111)$	8
Np(2)	−0.0243(2)	0	0.25	1	0.018(1)	2(100)	24
N	0.397(4)	0.144(4)	0.382(5)	1	0.003(9)	1	48
				NpN			
Np	0	0	0	1	0.0059(2)	$m3m$	4
N	0.5	0.5	0.5	1	0.0059(2)	$m3m$	4

dx.doi.org/10.1021/ja209503n | J. Am. Chem. Soc. 2012, 134, 3111−3119

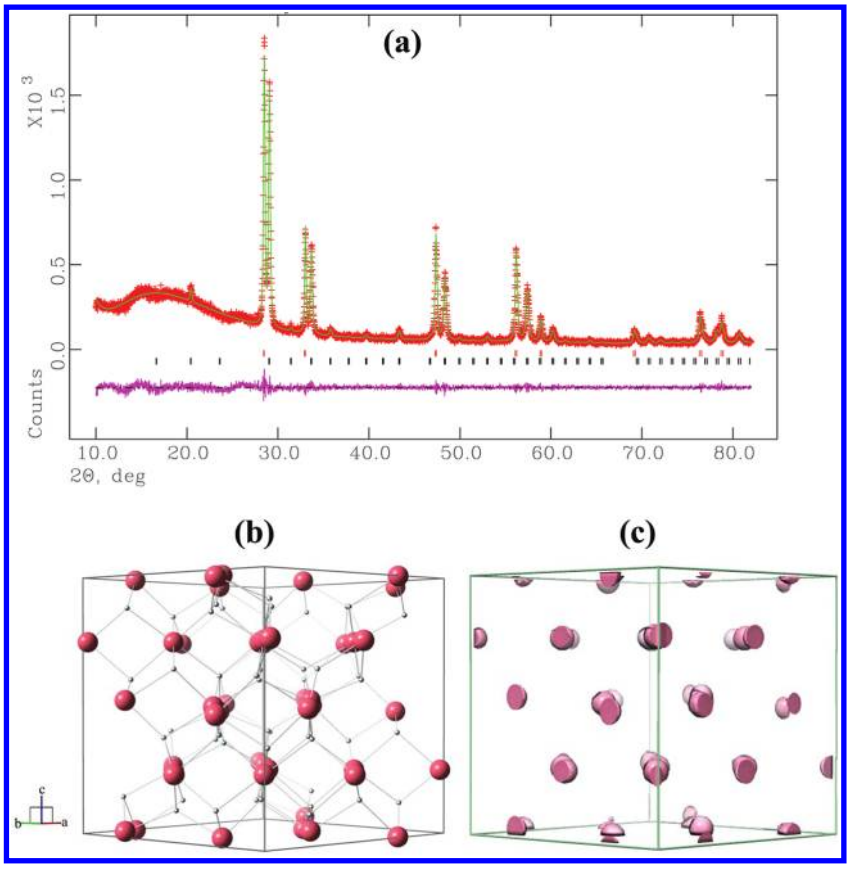

Figure 2. (a) The Rietveld analysis of the XRD pattern of the products formed after heating $(NH_4)Np_xF_y$ at 800 °C for 90 min using an open container (Np_2N_3 = 51.4 wt %, NpO_2 = 48.6 wt %, and χ^2 = 0. 93). The lower tick marks (black) represent reflections corresponding to Np_2N_3, while upper ones are of NpO_2. The large and amorphous-type broad peak at low 2θ of the XRD pattern was due to the Kapton tape used to seal the sample. (b) A ball-and-stick model of the refined Np_2N_3 unit cell. (c) Electron density map of Np_2N_3 unit cell (only the Np atomic sites are shown using a 3.1 level of display).

Np(1) and Np(2), in Table 2. Each of these two neptunium atoms forms bonds with six nitrogen atoms, resulting in complexly packed polyhedra. The Np(1)−N bond lengths are identical to a value of 2.39(7) Å, while Np(2)−N bonds consist of three different bond length values as given in Table 3.

Table 3. Selected Interatomic Distances and Angles for NpN_x

distances (Å)		angles (deg)	
		NpN_2	
Np−N	2.305	N−Np−N	70.5
		N−Np−N	109.5
		Np_2N_3	
Np(1)−N	2.39(7)	N−Np(1)−N	101.7(9)
Np(2)−N	2.24(3)	N−Np(2)−N	106(3)
Np(2)−N	2.37(4)	N−Np(2)−N	75(2)
N−Np(2)	2.19(1)	N−Np(2)−N	76(2)
		Np(1)−N−Np(2)	102(2)
		Np(1)−N−Np(2)	98(2)
		Np(2)−N−Np(2)	102(2)
		NpN	
Np−Np	3.465	N−Np−N	180.0
Np−N	2.449	Np−N−Np	90

An electron density map of the Np_2N_3 unit cell calculated using charge flipping method is shown in Figure 2c. Only the high electron density corresponding to neptunium atomic sites is shown in this figure. The well-matched electron densities to neptunium lattice points represented in Figure 2b confirmed the Np_2N_3 crystal structure to be isomorphous to U_2N_3 of $Ia\bar{3}$ type crystal system.

3.3. Synthesis and Characterization of NpN. To minimize the further contamination of the system by oxygen, the synthesis of NpN was performed in a continuous two-step reaction. This two-step reaction involved first the ammonolysis of the ammonium−neptunium fluorides followed by the reduction of the higher nitrides into mononitride under inert atmosphere.

The first few attempts of making NpN using the ammonolysis of the reactants at 800 °C followed by the reduction at 1100 °C produced NpN with a low yield (Table 4). Performing the reduction step at lower temperatures, up to 800 °C, did not produce the expected NpN possibly because the NH_4−Np−F did not convert into higher nitrides (NpN_x). Ammonolysis followed by reduction at 900 °C produced NpN of reasonable phase purity. If the time of reduction step was lowered, even at 900 °C, full reactant conversions into the nitrides were not observed. At 900 °C, the lowest time of heating taken for the second step of the reaction was 45 min. Therefore, the reduction step was carried out up to 1100 °C to produce considerably higher (90 wt %) phase purity with acceptable levels of the oxide secondary phase for characterization. Given the small amount of reactants used and the high susceptibility of higher NpN_x chemical phases to oxygen, a single-phased NpN was not able to be produced using these

dx.doi.org/10.1021/ja209503n | J. Am. Chem. Soc. 2012, 134, 3111−3119

Table 4. Two-Step Conversion of NH_4−Np−F

under NH_3(g)		under inert atmosphere		products (wt %)		
temp (°C)	time (min)	temp (°C)	time (min)	NpN	NpO_2	other
800	90	800	60		53.5	NpN_2 (0.6); NpNF (45.9)
800	90	1100	30	16.3	83.7	
800	60	1100	15		87.9	NpF_3 (12.1)
800	90	1100	15		91.9	NpF_3 (8.1)
900	30	900	60	26.5	73.5	
900	30	900	30	23.9	37.5	NpNF (38.6)
900	30	900	45	61.9	38.1	
900	30	1100	30	90.0	10.0	

experimental conditions. The powder XRD analysis using the Rietveld method of the highest phase purity sample of NpN produced with the given experimental conditions is shown in Figure 3. The lattice parameter of the refined unit cell was 4.8999(1) Å, and the X-ray volume was 117.64(1) $Å^3$. These values were only slightly different (difference <0.1%) from that of the 62 wt % NpN sample (4.8961(1) Å and 117.37(1) $Å^3$). The refined lattice parameter for the synthesized NpN and unit-cell volume were also matched well with the reported values of 4.897(2) Å and 117.43 $Å^3$ (ICSD pattern # 31717), respectively.

3.4. Characterization of NpN_2, Np_2N_3, and NpN Using DFT. Total-energy calculations for the NpN_2, Np_2N_3, and NpN cubic phases were carried out from first-principles at the GGA +U level of theory for nonmagnetic (NM), ferromagnetic (FM), and antiferromagnetic type-I (AFM-I) solutions. For the three phases studied, the ground state is found to be FM, slightly more favorable energetically than the AFM-I and NM solutions. The total-energy differences $E_{FM} - E_{AFM}$ and $E_{FM} - E_{NM}$ per formula unit (f.u.) are 0.07 and 0.08 eV for NpN_2, 0.50 and 0.95 eV for Np_2N_3, and 0.08 and 0.38 eV for NpN, neglecting the on-site Coulomb repulsion. This appears to be consistent with the experimental observation of a FM ground state for NpN at low temperatures.[44] For the sake of simplicity, only FM results will be discussed in the rest of this study unless otherwise stated.

The variations of the lattice parameter, a_0, of the NpN_2, Np_2N_3, and NpN ferromagnetic structures as a function of the effective Hubbard parameter, U_{eff}, computed at the LDA+U and GGA+U levels of theory are shown in Figure 4; the experimental values of a_0 are also represented for comparison purpose. Typical of strongly correlated systems, the lattice parameters calculated with standard DFT within both the LDA and the GGA (U_{eff} = 0 eV) largely underestimate experimental values. Lattice parameters calculated with LDA+U are systematically shorter by ca. 0.1 Å than with GGA+U, due to the overbinding character of LDA as compared to GGA. The agreement between calculated and measured a_0 improves steadily as U_{eff} increases, with optimal values for GGA+U (LDA +U) corresponding to ca. 3 eV (5 eV) for NpN_2, 1 eV (4 eV) for Np_2N_3, and 1 eV (2 eV) for NpN. A monotonic decrease of the optimal U_{eff} value from the Np:N stoichiometry 1:2 to 1:1 is observed. Lattice parameters calculated with GGA+U with the optimal U_{eff} values given above are 5.32 Å for NpN_2, 10.64 Å for Np_2N_3, and 4.91 Å for NpN; these values will be used in the rest of the study unless otherwise stated.

The effects of the spin−orbit coupling (SOC) in the GGA +U calculations have also been studied for NpN_2 and NpN. The inclusion of SOC does not affect significantly the lattice parameters, slightly contracted by about 0.01 Å to 5.31 Å for NpN_2 and 4.90 Å for NpN. However, SOC is of crucial importance, together with on-site U_{eff} interaction corrections, for the accurate determination of the total energy and electronic and magnetic properties. The GGA+U total energies of NpN_2 and NpN calculated with SOC are lowered by 3.11 and 4.20 eV/f.u., respectively, as compared to the values obtained from collinear calculations. The magnetic moments per Np atom computed including SOC are M = 1.9 and 1.6 μ_B in NpN_2 and NpN, respectively, lower than the corresponding values without SOC, that is, M = 2.0 and 3.4 μ_B. The magnetic moment of Np in NpN computed with SOC is in good agreement with the experimental value of 1.4 ± 0.1 μ_B at 5 K

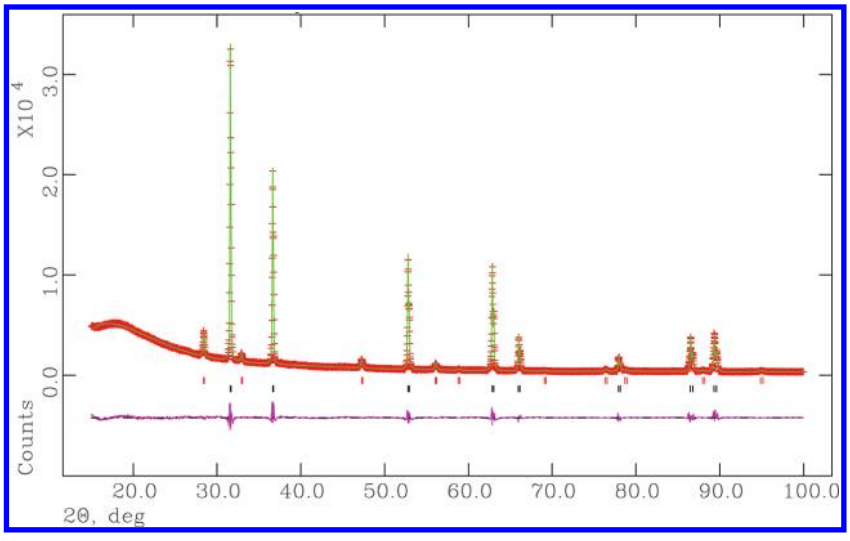

Figure 3. The Rietveld analysis of NpN (NpN = 90.0 wt %, NpO_2 = 10.0 wt %, and χ^2 = 2.20). This sample was synthesized heating $(NH_4)Np_xF_y$ at 900 °C for 30 min under NH_3(g) followed by 30 min at 1100 °C in an inert atmosphere. The lower tick marks (black) represent reflections corresponding to NpN, while upper ones are of NpO_2. The large and amorphous-type broad peak at low 2θ of the XRD pattern was due to the Kapton tape used to seal the sample.

dx.doi.org/10.1021/ja209503n | J. Am. Chem. Soc. 2012, 134, 3111−3119

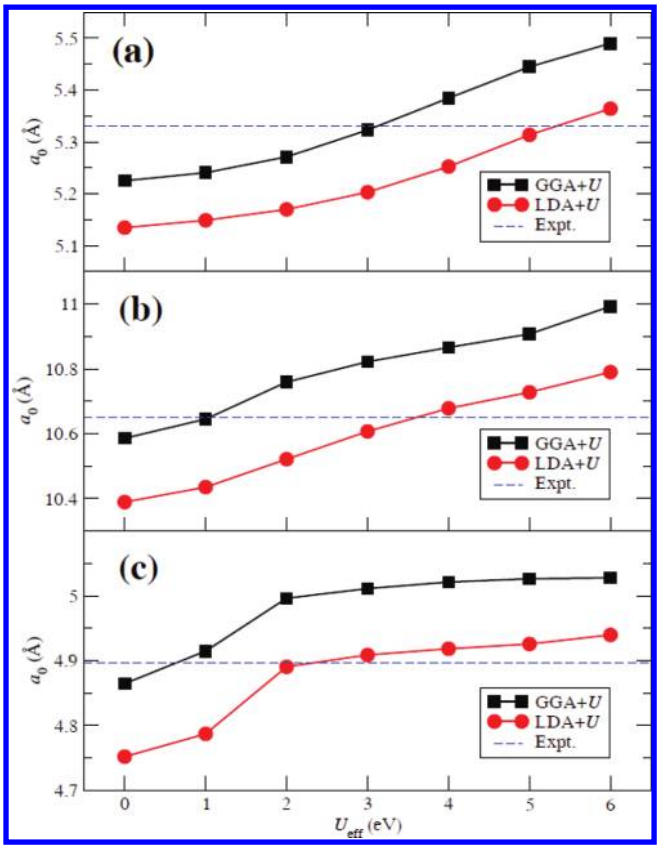

Figure 4. Variations of the lattice parameter, a_0, of the ferromagnetic (a) NpN_2 (space group $Fm\bar{3}m$, IT no. 225), (b) Np_2N_3 (space group $Ia\bar{3}$, IT no. 206), and (c) NpN (space group $Fm\bar{3}m$, IT no. 225) structures as a function of the effective Hubbard parameter, U_{eff}, computed at the LDA+U/PWC and GGA+U/PW91 levels of theory. Experimental values of a_0 are represented by dashed lines.

and represents a significant improvement over previously computed results.[25,26]

Density-of-states calculations for the equilibrium structures of NpN_2 and NpN have also been performed within the standard GGA, as well as within GGA+U with and without SOC (cf., Figure 5). For NpN, results are overall reminiscent of DOSs calculated in previously studies,[25,26] with N 2p states contributing to the total DOS between −6 and −1 eV and Np 5f character dominating near the Fermi level in the −1 to 4 eV energy range; other Np (6s,7s,6p,6d) and N 2s states do not appear to contribute significantly near the Fermi level, although Np 6d and 7s orbitals tend to hybridize with N 2p, and will be discarded in the rest of the discussion. The DOSs in Figure 5d,e (U_{eff} = 0 and 1 eV) show that the metallic character of NpN is due essentially to Np 5f majority spins, which contribute predominantly between −1 and 1 eV, while Np 5f minority spins dominate above 1 eV. The introduction of the parameter U_{eff} = 1 eV separates further apart the peaks corresponding to the f manifold. As shown in Figure 5f, the inclusion of the SOC, which lifts the degeneracy between Np $5f_{5/2}$ and $5f_{7/2}$, results in strong changes in the DOS; that is, contributions from Np 5f majority and minority spins become almost equivalent/symmetrical in the vicinity of the Fermi level. For NpN_2, DOS calculations show a larger degree of delocalization of 5f states, which extend from ca. −4 to 3 eV, as compared to 5f states in NpN, which tend to be localized near the Fermi level. The presence of a larger number of N 2p electrons available in NpN_2 as compared to NpN also leads to a stronger Np 5f−N 2p hybridization responsible for the delocalization of 5f states. The DOSs in Figure 5a,b (U_{eff} = 0 and 3 eV) suggest that NpN_2 is half-metallic, because only Np 5f majority spins are present at the Fermi level, while energy gaps of 0.8 (U_{eff} = 0 eV) and 1.9 eV (U_{eff} = 3 eV) open up for Np 5f minority spins. However, the DOS calculations including the SOC predict that NpN_2 is actually metallic, with both 5f majority and minority spins contributing almost equally near the Fermi level.

4. DISCUSSION AND CONCLUSIONS

Solid-phase conversion of the ammonium neptunium fluorides under NH_3(g) at different temperatures formed a series of neptunium compounds together with new species identified for the first time. At temperatures below 800 °C, ammonium neptunium fluorides decomposed into other stoichiometric ammonium neptunium fluorides such as $(NH_4)_2NpF_6$ and $NH_4Np_3F_{13}$ (Table 1). At temperatures in excess of 800 °C and with enough time of heating applied, further decomposition of the ammonium neptunium fluorides was observed. NpN_xF_y and two other novel nitrides (NpN_2 and Np_2N_3) were produced under these experimental conditions. The two new neptunium nitride compounds, NpN_2 and Np_2N_3, were found to be isomorphous with UN_2 and U_2N_3, respectively, based on the powder XRD studies.

NpN_2 crystallizes in a face-centered cubic ($Fm\bar{3}m$) crystal system with 5.3236(1) Å lattice parameter and 150.871(5) Å^3 unit cell volume. This unit cell consists of 14 lattice points of Np identical to each other. Eight of them are at unit cell corners, while the other six are located at the centers of the 6 unit cell faces. Each of these 6 Np atoms forms bonds with 4 N atoms defining polyhedra within the cell. Eight N atoms in the unit cell participate in the Np−N bonding. The body-centered cubic ($Ia\bar{3}$) crystal system of the Np_2N_3 is characterized by a 10.6513(4) Å lattice parameter and a 1208.4(1) Å^3 volume. The large Np_2N_3 unit cell consists of 44 lattice points corresponding to two different environments of neptunium atoms. Each of these atoms forms bonds with six nitrogen atoms.

High and low electron densities in the NpN_2 unit cell atomic sites corresponding to the heavy Np and light N atoms, respectively, were observed by charge flipping calculations. These electron density maps matched well with the lattice points of the refined NpN_2 unit cell, confirming the crystal structure identified with powder XRD analysis. The electron densities calculated with charge-flipping also matched the heavy atomic sites of neptunium in the Np_2N_3 unit cell, confirming the unit cell symmetry used for Rietveld analysis.

The crystal structures of NpN_2 and Np_2N_3 were further confirmed by density functional calculations performed within the local-density approximation (LDA+U) and the generalized-gradient approximation (GGA+U) corrected with an effective Hubbard parameter to account for the strong on-site Coloumb repulsion between Np 5f electrons. The effects of the spin−orbit coupling (SOC) in the GGA+U calculations were investigated for NpN_2 and NpN; it was found that SOC is necessary for the calculations of accurate electronic and magnetic properties in the Np−N system. Density of states calculations show a larger degree of delocalization of 5f states in NpN_2, as compared to 5f states in NpN, which tend to be localized near the Fermi level, due to a stronger Np 5f−N 2p hybridization.

dx.doi.org/10.1021/ja209503n | J. Am. Chem. Soc. 2012, 134, 3111−3119

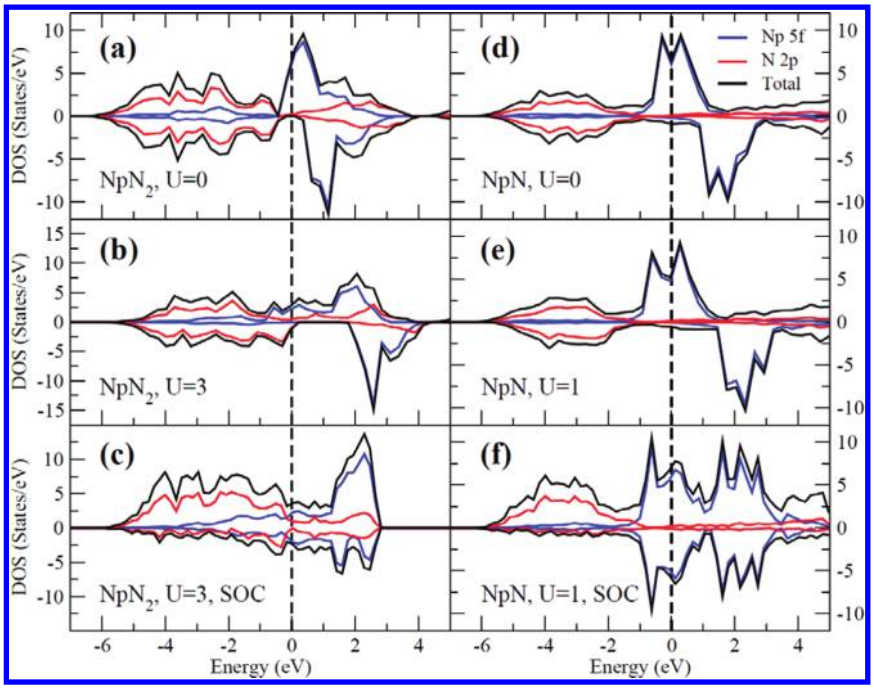

Figure 5. Total and orbital-projected densities of states (DOSs) of the ferromagnetic NpN_2 (left column) and NpN (right column) phases computed at the GGA and GGA+*U* levels of theory. The DOSs represented correspond to standard GGA with U_{eff} = 0 eV (top), optimal U_{eff} = 3 and 1 eV values for NpN_2 and NpN (middle), and optimal U_{eff} values with inclusion of spin−orbit coupling (bottom). Color legend: Np 5f, blue; N 2p, red; total DOS, black. Positive and negative values of the DOSs correspond to majority and minority spins, respectively. The Fermi level is set to zero (dashed lines).

Synthesis of NpN using this low-temperature fluoride route was also successful. NpN was synthesized at temperatures from 900 to 1100 °C. In examining the reaction products, it was hypothesized that the secondary oxide phases were formed through reactions of the converted nitrides with trace oxygen in the system at elevated temperatures.

In previous work with the uranium nitride system, sequential conversion of the ammonium uranium fluoride to the mononitride through ammonolysis to form UN_2 followed immediately by conversion to the mononitride under argon without cooling the sample between reaction steps produced a UN product of reasonable purity.[17] A similar approach for synthesizing single-phased NpN was not successful, most likely due to the small quantities of reactants used. However, even with the use of small quantities of reactant ammonium neptunium fluorides, it was demonstrated that phase purity of the NpN can be increased by lowering the reduction temperature or the time of heating at high temperatures such as 1100 °C. The NpN can be synthesized at temperatures ≤900 °C using the fluoride route discussed in this study. Future study on the neptunium system is therefore suggested using large amounts of reactants to optimize the reaction conditions to synthesize single-phased NpN using the fluoride route. It is also envisaged that this fluoride route be investigated for transuranium systems having high vapor pressures at elevated temperatures to synthesize AnN.

■ ASSOCIATED CONTENT

Supporting Information

Crystallographic information files (CIF) for neptunium dinitride (NpN_2) and neptunium sesquinitride (Np_2N_3). This material is available free of charge via the Internet at http://pubs.acs.org.

■ AUTHOR INFORMATION

Corresponding Author

silvagw@ornl.gov

Notes

The authors declare no competing financial interest.

■ ACKNOWLEDGMENTS

Sample synthesis and characterization was performed at the University of Nevada, Las Vegas (UNLV), under the UNLV Transmutation Research Program and was funded by the U.S. Department of Energy (Grant No. DE- FG07-01AL67358). Completion of this manuscript and final data analysis at Oak Ridge National Laboratory were sponsored by the U.S. Department of Energy Office of Nuclear Energy. Sandia National Laboratories is a multiprogram laboratory operated by Sandia Corp., a wholly owned subsidiary of Lockheed Martin Co., for the United States Department of Energy's National Nuclear Security Administration under Contract DE-AC04-94AL85000. We thank Dr. Anthony Hechanova for administrating the UNLV Transmutation Research Program, and Tom O'Dou and Trevor Low for laboratory management and radiation safety support for this work. We thank Dr. Bob Van Dreele at Los Alamos National Laboratory, U.S., and Nicola Ashcroft at International Union of Crystallography, England, for valuable discussions on XRD analysis that helped to improve the quality of this Article.

■ REFERENCES

(1) Mizutani, A.; Sekimoto, H. *Ann. Nucl. Energy* **1998**, *25*, 1011−1020.

(2) Arai, Y.; Nakajima, K.; Suzuki, Y. *J. Alloys Compd.* **1998**, *271−273*, 602.

(3) Suzuki, Y.; Arai, Y. *J. Alloys Compd.* **1998**, *271−273*, 577.

(4) Minato, K.; Akabori, M.; Takano, M.; Arai, Y.; Nakajima, K.; Itoh, A.; Ogawa, T. *J. Nucl. Mater.* **2003**, *320*, 18−24.
(5) Ogawa, T.; Akabori, M.; Kobayashi, F.; Haire, R. G. *J. Nucl. Mater.* **1997**, *247*, 215−221.
(6) Suzuki, Y.; Arai, Y. *J. Alloys Compd.* **1998**, *271*−*273*, 577−582.
(7) Arai, Y.; Nakajima, K.; Suzuki, Y. *J. Alloys Compd.* **1998**, *271*−*273*, 602−605.
(8) Rogozkin, B. D.; Stepennova, N. M.; Bergman, G. A.; Proshkin, A. A. *At. Energy* **2003**, *95*, 835−844.
(9) Srivastava, D.; Garg, S. P.; Goswami, G. L. *J. Nucl. Mater.* **1989**, *161*, 44−56.
(10) Streit, M.; Ingold, F. *J. Eur. Ceram. Soc.* **2005**, *25*, 2687−2692.
(11) Arai, Y.; Minato, K. *J. Nucl. Mater.* **2005**, *344*, 180−185.
(12) Yamawaki, M.; Inoue, T.; Ogawa, T. *Pure Appl. Chem.* **2000**, *72*, 1839−1849.
(13) Ross, S. B.; El-Genk, M. S.; Matthews, R. B. *J. Nucl. Mater.* **1990**, *170*, 169−177.
(14) Mathews, R. B.; Chidester, K. M.; Hoth, C. W.; Mason, R. E.; Petty, R. L. *J. Nucl. Mater.* **1988**, *151*, 334−344.
(15) Bauer, A. *React. Technol.* **1972**, *15*, 87−104.
(16) Yeamans, C. B.; Silva, G. W. C.; Cerefice, G. S.; Czerwinski, K. R.; Hartmann, T.; Burrell, A. K.; Sattelberger, A. P. *J. Nucl. Mater.* **2008**, *374*, 75−78.
(17) Silva, G. W. C.; Yeamans, C. B.; Sattelberger, A. P.; Hartmann, T.; Cerefice, G. S.; Czerwinski, K. R. *Inorg. Chem.* **2009**, *48*, 10635.
(18) Arai, Y.; Fukushima, S.; Shiozawa, K.; Handa, M. *J. Nucl. Mater.* **1989**, *168*, 280.
(19) Takano, M.; Akabori, M.; Arai, Y.; Minato, K. *J. Nucl. Mater.* **2008**, *376*, 114.
(20) Olson, W. M.; Mulford, R. N. R. *J. Phys. Chem.* **1966**, *70*, 2932.
(21) Sheft, I.; Fried, S. *J. Am. Chem. Soc.* **1953**, *75*, 1236.
(22) Grenthe, I.; Drozdzynski, J.; Fujino, T.; Buck, E. C.; Albrecht-Schmitt, T. E.; Wolf, S. F. In *The Chemistry of the Actinide and Transactinide Elements*, 4th ed.; Morss, L. R., Edelstein, N. M., Fuger, J., Eds.; Springer: Dordrecht, The Netherlands, 2011; pp407−411.
(23) Sedmidubsky, D.; Konings, R. J. M.; Novak, P. *J. Nucl. Mater.* **2005**, *344*, 40.
(24) Kurosaki, K.; Adachi, J.; Uno, M.; Yamanaka, S. *J. Nucl. Mater.* **2005**, *344*, 45.
(25) Atta-Fynn, R.; Ray, A. K. *Phys. Rev. B* **2007**, *76*, 115101.
(26) Suzuki, S.; Li, M.-F.; Ariizumi, T. *J. Phys. Soc. Jpn.* **2008**, *77*, 074703.
(27) Petit, L.; Svane, A.; Szotek, Z.; Temmerman, W. M.; Stocks, G. M. *Phys. Rev. B* **2009**, *80*, 045124.
(28) Shibata, H.; Tsuru, T.; Hirata, M.; Kaji, Y. *J. Nucl. Mater.* **2010**, *401*, 113.
(29) Silva, G. W. C.; Yeamans, C. B.; Ma, L.; Cerefice, G. S.; Czerwinski, K. R.; Sattelberger, A. P. *Chem. Mater.* **2008**, *20*, 3076−3084.
(30) Larson, A. C.; Von Dreele, R. B. General Structure Analysis System (GSAS). Los Alamos National Laboratory Report LAUR 86-748, 2004.
(31) DusIek, M.; PetrIoAcIek, V.; Wunschel, M.; Dinnebier, R. E.; Smaalen, S. *J. Appl. Crystallogr.* **2001**, *34*, 398−404.
(32) Le Bail, A.; Duroy, H.; Fourquet, J. L. *Mater. Res. Bull.* **1988**, *23*, 447−452.
(33) Palatinus, L.; Chapuis, G. *J. Appl. Crystallogr.* **2007**, *40*, 786−790.
(34) Pettersen, E. F.; Goddard, T. D.; Huang, C. C.; Couch, G. S.; Greenblatt, D. M.; Meng, E. C.; Ferrin, T. E. *J. Comput. Chem.* **2004**, *25*, 1605−1612.
(35) Kresse, G.; Furthmüller, J. *Phys. Rev. B* **1996**, *54*, 11169−11186.
(36) Perdew, J. P.; Chevary, J. A.; Vosko, S. H.; Jackson, K. A.; Pederson, M. R.; Singh, D. J.; Fiolhais, C. *Phys. Rev. B* **1992**, *46*, 6671−6687.
(37) Perdew, J. P.; Wang, Y. *Phys. Rev. B* **1992**, *45*, 13244−13249.
(38) Dudarev, S. L.; Botton, G. A.; Savrasov, S. Y.; Humphreys, C. J.; Sutton, A. P. *Phys. Rev. B* **1998**, *57*, 1505.
(39) Andersson, D. A.; Lezama, J.; Uberuaga, B. P.; Deo, C.; Conradson, S. D. *Phys. Rev. B* **2009**, *79*, 024110.
(40) Blöchl, P. E. *Phys. Rev. B* **1994**, *50*, 17953−179179.
(41) Kresse, G.; Joubert, D. *Phys. Rev. B* **1999**, *59*, 1758−1175.
(42) Methfessel, M.; Paxton, A. T. *Phys. Rev. B* **1989**, *40*, 3616−3621.
(43) Monkhorst, H. J.; Pack, J. D. *Phys. Rev. B* **1976**, *13*, 5188−5192.
(44) Aldred, A. T.; Dunlap, B. D.; Harvey, A. R.; Lam, D. J.; Lander, G. H.; Mueller, M. H. *Phys. Rev. B* **1974**, *9*, 3766.